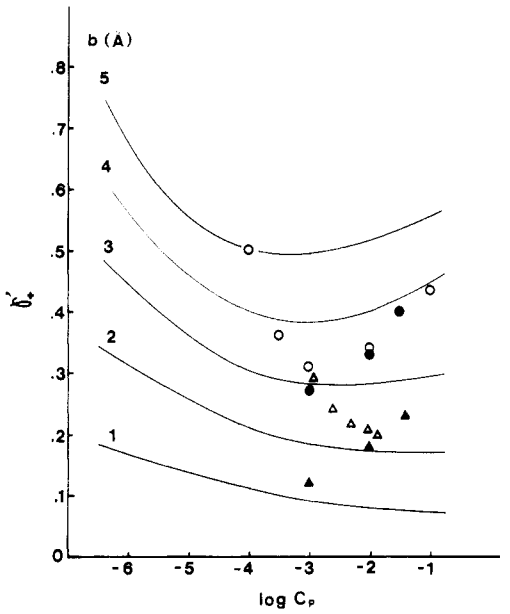

Figure 6. Comparison of experimental counterion activity coefficients for salt-free polyelectrolyte systems with the theoretical curves of eq 12. (○) NaPMSS,[25] $N = 761$ and $b = 2.66 \times 10^{-8}$ cm; (●) NaPVS,[14] $N = 293$ and $b = 5.8 \times 10^{-8}$ cm; (▲) NaPVS,[14] $N = 348$ and $b = 3.38 \times 10^{-8}$ cm; (△) AgCMC,[23] $N = 289$ and $b = 3.31 \times 10^{-8}$ cm. Theoretical curves: $N = 1000$.

solutions has been made without an explicit consideration of the condensed phase. Values of θ and γ thus obtained were compared with other theories and experimental data. The benefit of the present study may consist in that the dependences of θ and γ on C_s, C_p, and N can be predicted. Satisfactory agreements with the experimental data of Kowblansky et al.[5] were found for C_s and C_p dependences of γ/γ_0. A minor modification of our model[29] will extend the applicability to systems containing counterions with different valences and to those in which dehydrations from counterions and polyions are involved in the condensation process.

References and Notes

(1) Manning, G. S. *J. Chem. Phys.* **1969**, *51*, 924.
(2) Manning, G. S. *Q. Rev. Biophys.* **1978**, *11*, 179.
(3) Ise, N.; Okubo, T. *Macromolecules* **1978**, *11*, 439.
(4) Kwak, J. C. T.; O'Brien, M. C.; MacLean, D. A. *J. Phys. Chem.* **1975**, *79*, 2381.
(5) Kowblansky, M.; Tomasula, M.; Ander, P. *J. Phys. Chem.* **1978**, *82*, 1491.
(6) Joshi, Y. M.; Kwak, J. C. T. *Biophys. Chem.* **1981**, *13*, 65.
(7) Kwak, J. C. T.; Murphy, G. F.; Spiro, E. J. *Biophys. Chem.* **1978**, *7*, 379.
(8) Trifiletti, R.; Ander, P. *Macromolecules* **1979**, *12*, 1197.
(9) Guéron, M.; Weisbuch, G. *Biopolymers* **1980**, *19*, 353.
(10) Le Bret, M.; Zimm, B. H. *Biopolymers* **1984**, *23*, 287.
(11) Woodbury, C. P., Jr.; Ramanathan, G. V. *Macromolecules* **1982**, *15*, 82.
(12) Ramanathan, G. V.; Woodbury, C. P., Jr. *J. Chem. Phys.* **1982**, *77*, 4133.
(13) Iwasa, K. *Biophys. Chem.* **1979**, *9*, 397.
(14) Nagasawa, M.; Kagawa, I. *J. Polym. Sci.* **1957**, *25*, 61.
(15) Nagasawa, M. *J. Polym. Sci., Polym. Symp.* **1975**, *No. 49*, 1.
(16) Miyamoto, S. *Biophys. Chem.* **1979**, *9*, 79.
(17) Dolar, D.; Span, J.; Isakovic, S. *Biophys. Chem.* **1974**, *1*, 312.
(18) Schindewolf, U. *Z. Phys. Chem. (Frankfurt/Main)* **1954**, *1*, 134.
(19) Iwasa, K.; Kwak, J. C. T. *J. Phys. Chem.* **1977**, *81*, 408.
(20) Bratko, D.; Dolar, D. *J. Chem. Phys.* **1984**, *80*, 5782.
(21) Joshi, Y. M.; Kwak, J. C. T. *J. Phys. Chem.* **1979**, *83*, 1978.
(22) Delville, A. *Biophys. Chem.* **1984**, *19*, 183.
(23) Kagawa, I.; Katsuura, K. *J. Polym. Sci.* **1955**, *17*, 365.
(24) Nagasawa, M.; Izumi, M.; Kagawa, I. *J. Polym. Sci.* **1959**, *37*, 375.
(25) Oman, S.; Dolar, D. *Z. Phys. Chem. (Frankfurt/Main)* **1967**, *56*, 1.
(26) Fernandez-Prini, R.; Lagos, A. E. *J. Polym. Sci.* **1964**, *2*, 2917.
(27) Fernandez-Prini, R.; Baumgartner, E.; Liberman, S.; Lagos, A. E. *J. Phys. Chem.* **1969**, *73*, 1420.
(28) Lubas, W.; Ander, P. *Macromolecules* **1980**, *13*, 318.
(29) Satoh, M.; Komiyama, J.; Iijima, T., in preparation.

Dye Binding Characteristics of Imidazole-Containing Polymers

T. M. Handel, H. L. Cohen, and J. S. Tan*

Research Laboratories, Eastman Kodak Company, Rochester, New York 14650.
Received September 26, 1984

ABSTRACT: The interactions of methyl orange with methyl, hexyl, and benzyl quaternized poly(*N*-vinylimidazoles) were studied to assess the structural factors and the nature of the driving forces for dye binding. The stoichiometry of the polymer–dye complex is dictated by charge. The apparent binding constant increases with polymer charge density as well as polymer saturation r (where $r = [D_b]/[P_t]$, and $[D_b]$ and $[P_t]$ are the molar concentrations of bound dye and total polymer quaternary sites, respectively), but decreases in the presence of competing counterions, indicating that Coulombic forces operate. The van der Waals forces between the dye and the aromatic or long-chain hydrocarbon group at the polymer quaternary site also enhance binding strength. Cooperative dye binding was observed in the region $0 \leq r \leq 0.7$. This behavior is discussed in terms of the dimerization tendency of the dye molecules. In the high-saturation region ($0.7 \leq r \leq 1.0$), however, steric hindrance prevents further aggregation of the dye, and cooperativity was lost.

Two types of interactions can occur between an aromatic dye molecule and a polymer in aqueous solution, i.e., the nonspecific adsorption and the specific site interaction. The former interaction is a result of van der Waals attraction between molecules caused by dipole–dipole, dipole–induced dipole, and the London dispersion forces. The enthalpy of such an interaction is generally very small among nonpolar linear hydrocarbons, but the total free energy change in an aqueous medium can be significant because of an entropy gain resulting from the structural change of the "hydrophobic hydration"[1] shells surrounding the associated complex.[2,3] The second type of interaction involves specific sites on the polymer where a covalent bond, metal complex, charge-transfer complex, or ion-pair formation takes place. The enthalpy for this type of interaction is generally large, and the total free energy change may be enhanced by an entropy gain caused by the "hydrophobic effect"[2,3] described above for the nonspecific nonpolar association.

The interaction between anionic dye molecules and synthetic polycations has been investigated by several workers,[4-8] yet the nature of the driving forces for binding,

0024-9297/85/2218-1200$01.50/0

Table I
Structures of Methyl Orange and Polymers

Compound	Structure	Symbol
Methyl Orange	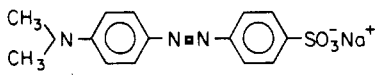	MO
Homopolymers		PVI
	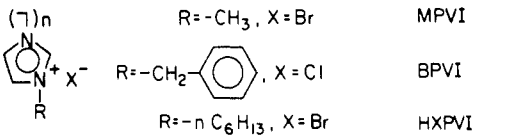	MPVI
		BPVI
		HXPVI
Copolymers	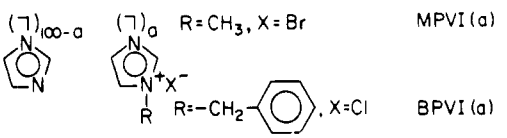	MPVI(a)
		BPVI(a)

the molecular mechanisms for the binding process, the stoichiometries, and the geometries of the bound complexes cannot be generalized. To gain such molecular insight, we chose to study methyl orange and several homopolymers and copolymers containing imidazole and imidazolium salts.

In this work, we investigated the effects of polymer structure (such as the type of the quaternizing groups and the extent of quaternization) and the competing counterions on dye binding characteristics. The binding data were analyzed by the cooperative models involving bound dye–dye interactions. Other papers[9,10] discuss thermodynamic functions of dye binding, $\Delta G°$, $\Delta H°$, and $\Delta S°$, and a molecular mechanics model for estimating the relative magnitudes of the Coulombic and van der Waals interaction energies and the probable molecular geometries of the polymer–dye complexes.

Experimental Section

A. Materials. The structures of the polymers and the dye are shown in Table I. The preparations of poly(*N*-vinylimidazole) (PVI) and poly(3-benzyl-1-vinylimidazolium chloride) (BPVI) have been reported.[11]

The syntheses of the partially quaternized BPVI polymers, the homopolymer poly(3-methyl-1-vinylimidazolium bromide) (MPVI) and its partially quaternized forms, and the homopolymer poly(3-hexyl-1-vinylimidazolium bromide) (HXPVI) are described below.

1. Partially Quaternized Poly(3-benzyl-1-vinylimidazolium chloride). Five levels of quaternization were achieved by reacting PVI with different amounts of benzyl chloride for the same amount of polymer. For example, a sample containing 70 mol % quaternized groups was prepared as follows: To a solution of 1.0 g (1.1 mmol) of PVI in 15 mL of methoxyethanol was added 1.8 g (1.42 mmol) of benzyl chloride, and the mixture was heated for 2 days in a 60 °C bath. The solution was then treated with 1.8 g (0.75 mmol) of a 25% methanolic trimethylamine solution to react with the excess benzyl chloride. The solution was allowed to stand for 2 days at room temperature, dialyzed against distilled water for 4 days, and freeze-dried: yield 1.66 g.

The mole fraction of the monomer unit quaternized was smaller than the feed ratio. Two samples with 23% and 45% quaternization [BPVI(23) and BPVI(45)] were chosen for the present study.

2. Poly(3-methyl-1-vinylimidazolium bromide). Methyl bromide (96 g, 1 mol) was added to a solution of poly(*N*-vinylimidazole) (37.6 g, 0.4 mol) in *N,N*-dimethylformamide (200 mL) at room temperature under nitrogen. Upon precipitation of the polymer, additional *N,N*-dimethylformamide (100 mL) was added, and the mixture was stirred overnight. The mixture was then heated at 70–80 °C for 2 h under nitrogen. The solid was filtered and immediately dissolved in 300 mL of methanol to make a solution containing 25.6% solids. Additional methyl bromide (50 g, 0.5 mol) was added, and the solution was stirred overnight at room temperature. The polymer was precipitated with ethyl acetate, filtered, washed, and dried, yielding 68 g of solid material. Anal. Calcd for $C_6H_9N_2Br$: C, 38.1; H, 4.8; N, 14.9; Br, 42.2. Found: C, 37.3; H, 5.3; N, 14.7; Br, 40.3. 14.7; Br, 40.3.

3. Partially Quaternized Poly(3-methyl-1-vinylimidazolium bromide). A stoichiometric amount of gaseous methyl bromide was condensed into a solution of poly(*N*-vinylimidazole) in 150 mL of methoxyethanol at 0 °C. The solution, enclosed in a bomb, was heated overnight in a 60 °C bath. The absence of residual pressure in the vessel showed complete reaction of the methyl bromide. The solution was diluted to 600 mL with water, dialyzed, and freeze-dried. Two samples with 32% and 78% quaternization [MPVI(32) and MPVI(78)] were used.

4. Poly(3-hexyl-1-vinylimidazolium bromide). A solution of 10 g of poly(*N*-vinylimidazole) and 20 g of 1-bromo-*n*-hexane in 110 mL of methoxyethanol was heated in a steam bath for 48 h. The product was precipitated with ether, washed, and dissolved in 50 mL of methanol without drying. The product was again precipitated with ether, washed, and vacuum dried, giving 20 g of solid. Anal. Calcd for $C_{11}H_{19}NBr$: C, 51.0; H, 7.38; N, 10.8; Br, 30.8. Found: C, 49.4; H, 7.1; N, 10.5; Br, 28.1.

The dye, methyl orange (MO), was obtained from Kodak Laboratory Chemicals and purified by recrystallization.

B. Polymer Characterization. All polymers except HXPVI(Br) are water soluble and were dialyzed for 3 days and freeze-dried before use. The water-insoluble HXPVI(Br) polymer was dissolved in methanol and dialyzed against water. A uniform stable aqueous dispersion was obtained. The percentage of quaternization of the polymers was determined by acid–base titration of the imidazole groups and halide titration of the counterions associated with the quaternized groups.

The fractionation and characterization by intrinsic viscosity and light scattering of the BPVI homopolymer were reported elsewhere.[11] By using two fractions of fully quaternized BPVI (I_5, $\bar{M}_w$ = 470000; I_6, $\bar{M}_w$ = 180000), we showed that dye binding is independent of molecular weight. Consequently, all other polymers (Table II) were used in unfractionated form. Weight-average molecular weights for these polymers were determined by light scattering in MeOH/0.01 M tetrabutylammonium bromide solution.

Solution concentrations of all polymers are based on moles of quaternized sites (or the repeat unit in the case of the uncharged PVI) per liter. The concentrations of the stock polymer solutions were determined by weight and confirmed by titration of the counterions of the quaternized group.

In the following dye-binding measurements, the concentrations of the polymers were kept much smaller than the electrolyte concentrations so that complete counterion exchange was expected. Therefore, the nature of counterions in the original polymers should have little effect on the binding data.

C. Methods. 1. Spectrophotometric Titrations. A 3-mL portion of dye ([D] = 3.5×10^{-5}M) in aqueous 0.01 M NaAc was titrated with microliter increments of polymers ([P] = 0.01–0.03 M), and the spectra were recorded with a Varian Superscan 3 UV–visible spectrophotometer.

2. Equilibrium Dialysis. An 11-cm-long (1.5-cm diameter) cellulose tubing was soaked successively in MeOH/H_2O and

Table II
Intrinsic Viscosities (dL/g) as a Function of Salt Solution

		[η]		
polymer	$\bar{M}_w$	NaAc[a]	NaCl[a]	NaSCN[a]
BPVI(Cl)	470000	1.91	1.49	(ppt)
HXPVI(Br)[b]	1290000	3.75	3.05	(ppt)
MPVI(Br)	375000	3.28	2.78	2.3
PVI	210000		0.65	0.55

[a] 0.01 M. [b] The stock solution of the aqueous dispersion of HXPVI(Br) became clear when dissolved in 0.01 M NaAc or NaCl solutions.

Table III
Turbidimetric Titration

polymer	$\bar{M}_w$	[NaAc], M	[NaCl], M	[NaSCN], M
BPVI(Cl)	470 000	1.12	0.096	0.000 83
HXPVI(Cl)[a]	1 070 000	0.74	0.044	0.001 47
MPVI(Br)	375 000			0.063
PVI	210 000			

[a] Ion exchange was necessary to convert the water-insoluble HXPVI(Br) to water-soluble HXPVI(Cl).

demineralized H_2O for several days before use. Polymer and dye solutions used in the dialysis experiments were prepared in a minimum of 0.01 M aqueous salt to suppress the Donnan effect. The bags were filled with 10 mL of polymer solution with various concentrations (10^{-3}–10^{-5} M) and a magnetic stirrer, secured at both ends with polyester thread, and placed in a 30-mL beaker containing 10 mL of dye solution at a constant concentration (10^{-4} M). The beakers were covered and the solutions were allowed to equilibrate with stirring for 24 h. When binding was weak, additional experiments were run in which the polymer concentration was kept constant while the initial dye concentration outside the bag was varied (from 5×10^{-4} to 5×10^{-6} M). Blanks were run for each dye concentration to correct for the 1–3% adsorption of the dye by the bag.

Upon equilibration, free-dye concentrations were determined by measuring the absorbance of the dye solutions outside the bag. When the polymer concentrations were high, readings were taken at two intervals to ensure complete equilibration. The absorbance of the dye follows Beer's law over the concentrations used. The molar extinction coefficient of the dye in the aqueous solution was $2.72 \times 10^4 \pm 400$ cm^{-1} M^{-1} at 465 nm, in good agreement with that reported elsewhere.[6] The constancy of this coefficient in the different salt solutions warranted using this value at all times.

3. Intrinsic Viscosity. Intrinsic viscosities were measured in various salt solutions with a Ubbelöhde viscometer at 25 °C (see Table II). Details of the procedure were reported previously.[12] The BPVI, MPVI, and PVI polymers were soluble in the aqueous salt solutions studied. The stock solution of HXPVI(Br) dispersion was soluble in 0.01 M NaAc or NaCl.

4. Turbidimetric Titrations. A 3-mL portion of a 0.2–1% polymer solution was titrated with a concentrated salt solution by use of a microliter syringe. For the water-insoluble HXPVI(Br), counterion exchange gave water-soluble HXPVI(Cl). The salt concentration at the onset of turbidity (see Table III) was taken as a relative measure of counterion binding.[11] Turbidity was observed by the scattering of incident light from a microscope lamp on the solution.

5. Acid–Base Titration. A 15-mL portion of a 0.01 M (base moles) polymer solution in 50:50 MeOH/CH_3CN and 0.25 M tetrabutylammonium bromide was titrated with HCl. The pH was monitored with a Corning Model 130 pH meter and a Sargent-Welch miniature combination electrode.

6. Chloride Titration. The quaternized groups of the homopolymers were determined from titration of the halide counterion by incremental addition of 0.02 M $AgNO_3$ to 15 mL of an aqueous solution containing 2.5 mmol of polymer. The same procedure was followed for titration of the copolymers except that 2 equiv of HNO_3 per equivalent of imidazole monomer was added to avoid silver complexation with the base. A Corning Model 130 pH meter equipped with Orion silver and double-junction reference electrodes was used to measure the potential (millivolts) as a function of added $AgNO_3$.

Results and Discussion

A. Spectral Behavior. To determine the stoichiometry of the polymer–dye complex and probe the environment of the bound dye, we spectrophotometrically titrated MO with the various polymers. Figure 1 shows the titration curves for MO + BPVI in 0.01 M NaAc at various $[P_t]/[D_t]$ ratios, where $[P_t]$ is the total molar concentration of the polymer quaternized sites and $[D_t]$ is the total dye concentration. The absorption spectrum peaking at 465 nm corresponding to $[P_t]/[D_t] = 0$ is that of the isolated monomeric dye in the absence of polymer. Upon addition of polymer, the band at 465 nm gradually decreases in intensity and is replaced by a new band around 390 nm. From a plot of the absorbance at 465 nm vs. $[P_t]/[D_t]$, a complex stoichiometry of unity was obtained from the interpolated end point. Similar stoichiometry was also obtained for the other quaternized homopolymers, showing that complex composition is dictated by charge.

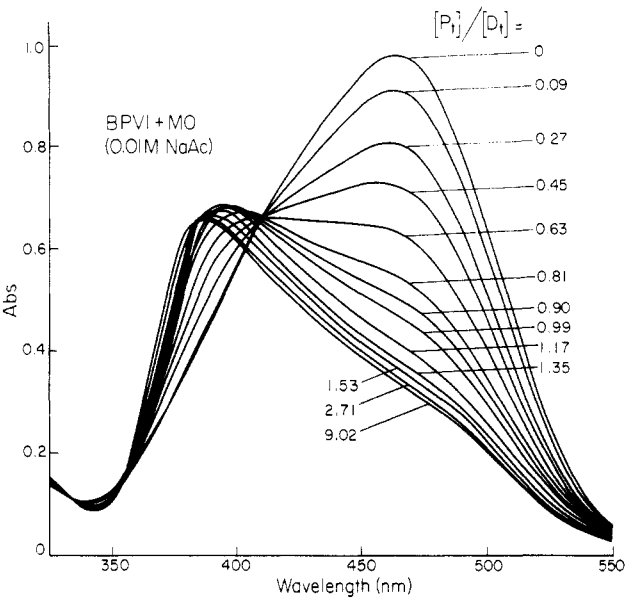

Figure 1. Spectral changes for MO + BPVI in 0.01 M NaAc at various $[P_t]/[D_t]$.

For the partially quaternized copolymers, the end points were slightly less than unity, e.g., $[P_t]/[D_t] = 0.8$ for MO + MPVI(32), suggesting some binding of the dye at the uncharged sites. However, these stoichiometries may be contrasted to the larger values found for uncharged polymers such as poly(vinylpyrrolidone),[13] again demonstrating the importance of charge for high binding capacity of the present polymers.

For MPVI and HXPVI with MO, the spectral curves with changing $[P_t]/[D_t]$ follow the same trend as that for BPVI. The curve shapes, however, are slightly different (Figure 2a). The new band that appears when the concentration of polymer is increased (at low $[P_t]/[D_t]$) is sharper and further blue shifted to 370 nm. Analogous spectral features were reported by others for MO bound to poly(vinyl-*N*-methylpyridinium chloride),[5] poly(L-lysine),[5] poly(L-ornithine),[5] acylated poly(ethylenimine),[4] and the methyl sulfate analogue of MPVI.[6]

Reeves and Harkaway explained the origin of the high-energy band (370 nm for MO + MPVI) from dye stacking on the polymer backbone.[6] This interaction between the bound dye molecules may also be accompanied by the additional interaction between the dye and pendant polymer groups (e.g., 390 nm for MO + BPVI), causing differences in the orientation of the stacked dyes. The transition moments of the excited chromophores may, therefore, vary with each polymer, resulting in the observed spectral features.

If dye stacking is the cause of the blue-shifted bands, increasing the probability for the dyes to spread out along the polymer chain by increasing $[P_t]/[D_t]$ should result in a gradual disapperance of the high-energy band and appearance of a "monomeric" band for the bound dye. The spectral curves for MO + MPVI at high $[P_t]/[D_t]$ indeed show this. Figure 2b shows that the band associated with the isolated monomeric bound dye is centered at 465 nm,

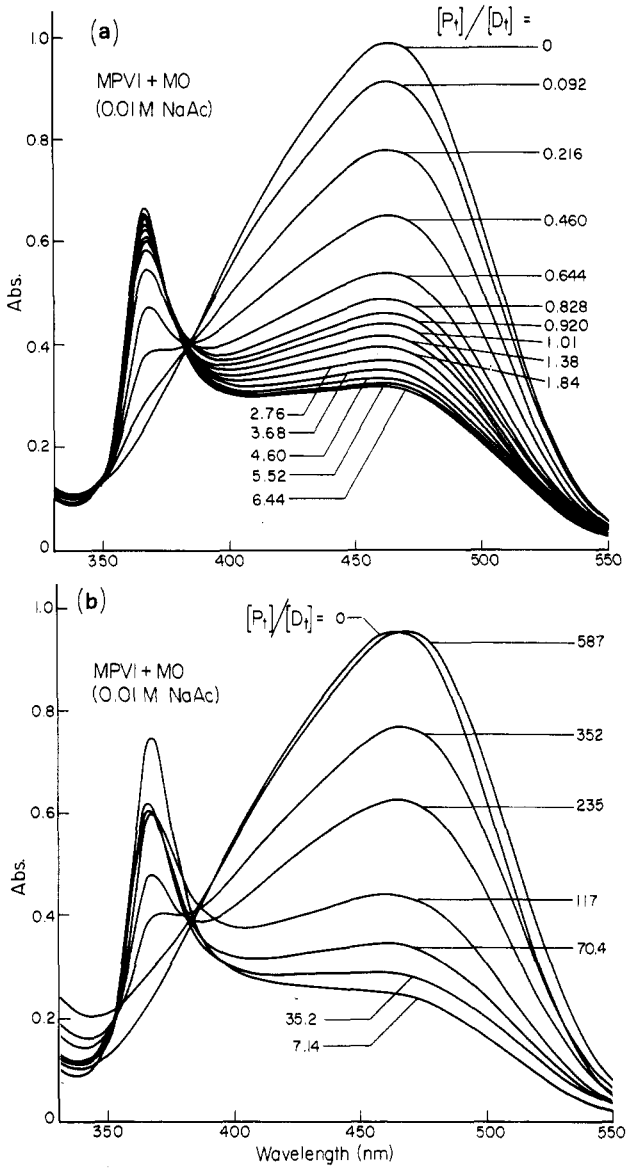

Figure 2. (a) Spectral changes for MO + MPVI in 0.01 M NaAc at low $[P_t]/[D_t]$. (b) Spectral changes for MO + MPVI in 0.01 M NaAc at high $[P_t]/[D_t]$.

similar to that for the free monomeric dye, and increases with increasing $[P_t]/[D_t]$ at the expense of the dye aggregate band at 370 nm. The large $[P_t]/[D_t]$ values necessary to recover the 465-nm band are noteworthy and may suggest cooperativity or a preference for the dye to occupy sites adjacent to bound dyes. Similar phenomena were observed for BPVI (data not shown) and the methyl sulfate analogue of MPVI.[6]

In addition to an estimation of the complex stoichiometries and insight into the nature of complexation, the equilibrium constant may be obtained from spectrophotometric titrations. This is possible, however, only for systems containing two absorbing species in equilibrium (i.e., free and bound dyes). In Figures 1 and 2 an isosbestic point, indicative of the presence of two species, persists only at low values of $[P_t]/[D_t]$. At higher values it is likely that the equilibrium involves several species, including free dye and various forms of bound dye. Consequently, the spectral change is too complex to be used for the analysis of the binding constant.

B. Effect of the Bound Dye–Dye Interaction on the Binding Isotherm. If all the binding sites are identical and binding at each site is independent of the binding at

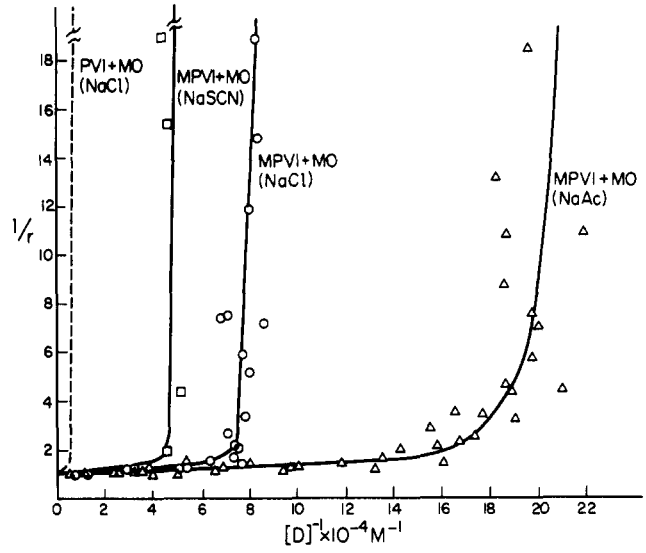

Figure 3. Klotz plots for MO + PVI (data points are outside the range of graph above $1/r = 18$) and MO + MPVI in 0.01 M NaAc, NaCl, and NaSCN.

other sites, the binding data can be described by any of the following equations:

$$\frac{1}{r} = \frac{[P_t]}{[D_b]} = \frac{1}{n} + \frac{1}{nK[D]} \quad \text{(Klotz[14] form)} \quad (1)$$

$$r/[D] = K(n - r) \quad \text{(Scatchard[15] form)} \quad (2)$$

$$r = nK[D]/(1 + K[D]) \quad \text{(Langmuir form)} \quad (3)$$

Here $[P_t]$ is the total molar concentration of the polymer binding sites (quaternized sites), $[D_b]$ and $[D]$ are the molar concentrations of the bound and free dye, n is the number of dyes bound per polymer site, and K is the intrinsic binding constant per pair of dye and binding site. A plot of $1/r$ vs. $1/[D]$ or $r/[D]$ vs. r according to eq 1 and 2, respectively, will be linear if binding obeys the above model. The binding constant may, therefore, be determined from the slope and the stoichiometry from the intercept.

In many cases, the occupation of one site on the polymer affects binding at neighboring sites so that K defined in eq 1–3 is no longer a true constant. Rather, it is dependent on the degree of occupation r of the polymer chain. The dissociation of polyacids and polybases shows a similar phenomenon.[16]

Figure 3 shows the Klotz plots for MO + PVI and MO + MPVI in various salt solutions. Because of weak binding, the data points for PVI are outside the range of the graph. The value of unity for $\lim_{[D]\to\infty} (1/r)$, as shown by the data points for the charged polymer MPVI + MO, indicates a complex stoichiometry of one, in agreement with the end point determined by spectrophotometric titrations discussed above. The nonlinearity of these plots suggests that eq 1 and 3 are not applicable because of interaction among the occupied sites, also consistent with the observed spectral shift previously discussed. Because of this neighboring site–site interaction, we shall use the apparent equilibrium constant K_{app} (per pair of dye–polymer site) defined as follows:

$$P + D \overset{K_{app}}{\rightleftharpoons} PD$$

where

$$K_{app} = \frac{[PD]}{[P][D]} = \frac{[D_b]}{\{[P_t] - [D_b]\}[D]} \quad (4)$$

In the following section, K_{app} will be presented as a

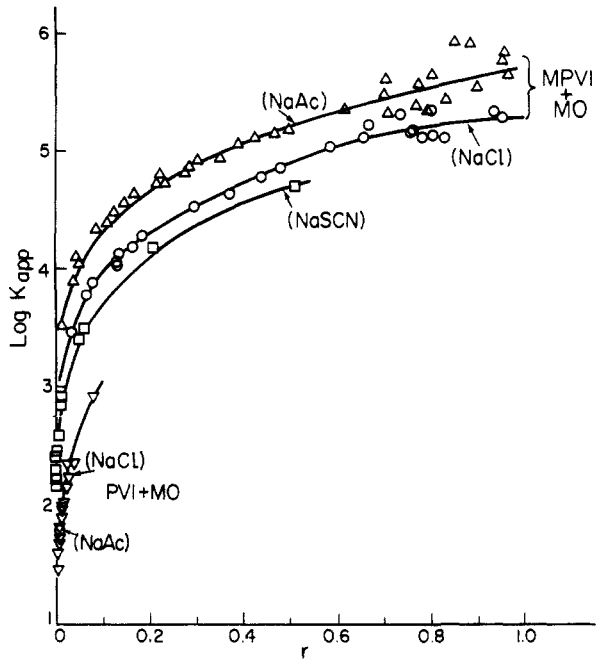

Figure 4. log K_{app} vs. r for MO + PVI and MO + MPVI in 0.01 M NaAc, NaCl, and NaSCN.

function of polymer saturation r for comparison of the binding strengths of the various polymers.

C. Effect of Quaternization and the Nature of the Quaternizing Side Chain on Binding Strength. The magnitude of K_{app} and how it varies with polymer saturation are shown in Figure 4 for the binding of MO to MPVI and PVI in various salt solutions (for PVI, $[P_t]$ is the concentration of monomer units). The increase in K_{app} with polymer saturation shows favorable interaction among the bound dye molecules.

The apparent equilibrium constant was measured only at low values of r for PVI because of the weak binding of this polymer and experimental difficulty of saturating the chain. For MPVI, the consistently higher values of K_{app} and the fact that binding data can be obtained for the fully occupied polymer (i.e., $r \rightarrow 1$) clearly show that quaternization enhances the binding strength and capacity substantially.

Although the plots for MO + MPVI showed curvature (Figure 3), linear Klotz plots for MO + BPVI and MO + HXPVI in 0.01 M NaCl and 0.01 M NaAc were obtained over the experimentally accessible concentration range (i.e., $0.8 < r < 1$). The linearity does not preclude interaction among the binding sites, however. Curvature corresponding to a decrease in binding strength with a decrease in r would be expected in the unsaturated region ($r < 0.8$), but binding data for this region are difficult to obtain for a strong binding polymer such as BPVI or HXPVI.

Linearity in the Klotz plots for MO + BPVI and MO + HXPVI in the concentration range ($0.8 < r < 1$) studied warrants calculation of a single value of K_{app} from the slope. For BPVI and HXPVI in 0.01 M NaAc, log K_{app} is 6.6 and 6.5, respectively. For MPVI in similar solvent conditions, log K_{app} corresponding to the saturated region ($r \rightarrow 1$ in Figure 4) is 5.7. The enhanced binding strength of the benzyl and hexyl quaternized polymers relative to MPVI results from additional nonionic forces between the dye and polymer side chain.

D. Effect of Counterion Binding on Dye Binding. To study the ionic component of polymer–dye interactions, we measured binding of the fully quaternized polymers and MO in various salt solutions. The polymer charge is screened and dye binding subsequently altered to a degree dependent on the extent of binding of the different counterions. Comparison of the relative extent of counterion binding to these polymers is shown by the data in Tables II and III. In the turbidimetric titrations (Table III) the concentration of a particular salt required to induce turbidity in the polymer solutions was taken as a relative measure of charge-screening ability. That is, the smaller the salt concentration required to induce turbidity, the stronger the counterion binding. For all the polymers, SCN^- is the most effective charge-screening counterion and Ac^- the least. The intrinsic viscosities in Table II corroborate the titration data. For a given polymer, a smaller intrinsic viscosity reflects a more tightly bound counterion and a highly collapsed chain. Again, the order of binding is $SCN^- > Cl^- > Ac^-$, which is similar to the order of the Hofmeister series for positively charged proteins.[17]

Figure 4 compares the effect of 0.01 M NaAc, NaCl, and NaSCN on the binding of MO to MPVI. The decrease in dye binding strength at a given r with increasing charge-screening ability of the counterion is what one would anticipate if Coulombic forces are important. Increasing the concentration of a given salt also decreases the dye binding strength in the same manner (data not shown). Similar ionic strength effects on dye binding strength were also observed for the BPVI and HXPVI polymers.

E. Effect of Charge Density on Dye Binding. In the preceding sections, we have demonstrated that quaternization enhances binding strength because of Coulombic as well as nonionic forces between the dye and the polymer side chain. These forces between the dye and a polymer site, however, may not be the only driving forces for the binding of MO with the polycations. The increase in K_{app} with r (Figure 4) and the blue shift of the dye absorption band upon binding of the dye to polymers shown earlier (Figures 1 and 2) suggest that bound dye–dye interaction may also contribute to the binding mechanism. This bound dye–dye interaction may be further examined by using PVI polymers quaternized to different extents so that the bound dye molecules are physically separated by the uncharged and weakly binding imidazole spacer groups. The apparent binding constants (per pair of dye–quaternary site) as defined by eq 4 are plotted against r in Figure 5a,b for the partially quaternized MPVI and BPVI, respectively. The effect of the bound dye–dye interactions on K_{app} is apparent from these data. The decrease in K_{app} with decreasing percentage quaternization, resulting from a decrease in bound dye–dye interaction, is substantiated in these data.

F. Cooperative Binding. Because the binding process for our systems cannot be described by the independent single-site model as discussed earlier (eq 1–3), we further examined our data by several interacting-site models.[14,15,18-22] Among them, the cooperative model proposed by McGhee and von Hippel is the most suitable for the present systems. The general reaction scheme and definition of binding constant are depicted in Figure 6. A cooperative interaction parameter ω has been incorporated in the binding constants for the singly contiguous site ($K_0\omega$) and the doubly contiguous site ($K_0\omega^2$). For a singly charged dye binding to one quaternary site on a partly saturated polymer, we use eq 5

$$\frac{r}{[D]} = K_0(1 - r)\left\{\frac{1 - 2r + R}{2(1 - r)}\right\}^2 \qquad (5)$$

where $R = \{(1 - 2r)^2 + 4\omega r(1 - r)\}^{1/2}$.

1. MPVI + MO. The binding data for MPVI + MO in 0.01 M NaCl are presented as the Scatchard plot in

Table IV
Binding Parameters for the Linear and Nonlinear Binding Regions according to the Klotz (Eq 1) and McGhee-von Hippel (Eq 5) Formulas

system	medium	r	n	log K (eq 6)	log K_0 (eq 16)	ω
MPVI + MO	0.01 M NaCl	$0.7 < r \leq 1.0$ (Klotz)	1	5.2		
		$0 \leq r \leq 0.7$ (McGhee-von Hippel)	1		2.85	100
BPVI + MO	0.05 M NaCl	$0.6 < r \leq 1.0$ (Klotz)	1	5.8		
		$0 \leq r < 0.6$ (McGhee-von Hippel)	1		4.0	55

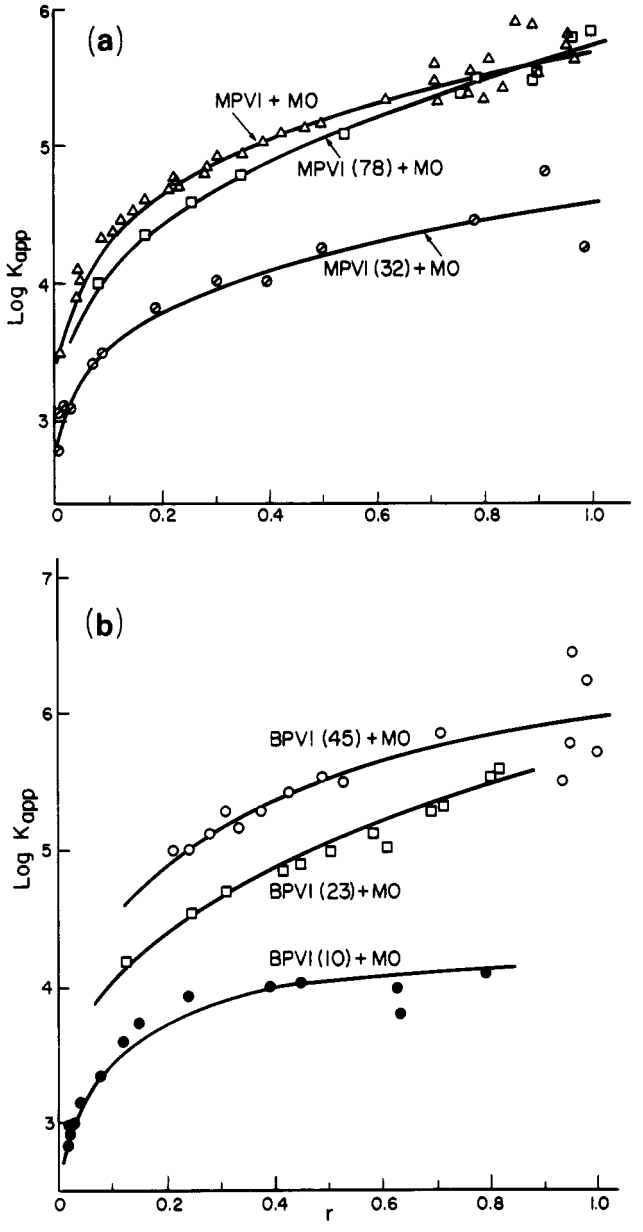

Figure 5. (a) log K_{app} vs. r for MO + MPVI as a function of percent quaternization. (b) log K_{app} vs. r for MO + BPVI as a function of percent quaternization.

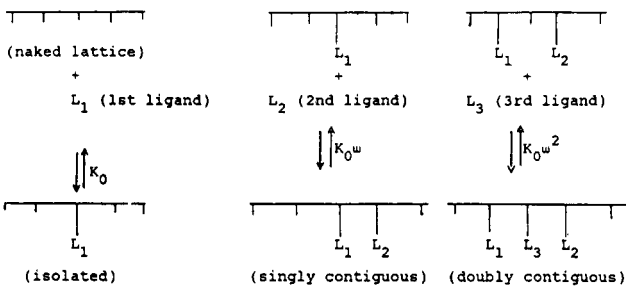

Figure 6. Reaction schemes for cooperative binding.

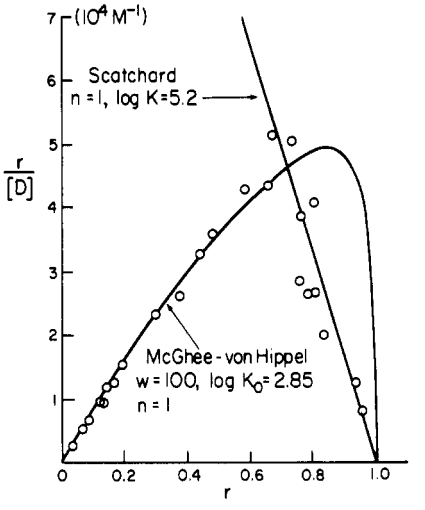

Figure 7. Scatchard plot $r/[D]$ vs. r for MPVI + MO in 0.01 M NaCl (solid curve: eq 5, $n = 1$, $\omega = 100$, log $K_0 = 2.85$; straight line: eq 2, $n = 1$, log $K = 5.20$; O: experimental data).

Figure 7. The theoretical curve that fits the data points in the lower region $0 \leq r \leq 0.7$ is calculated according to eq 5 by using the two parameters log $K_0 = 2.85$ and $\omega = 100$ obtained by iteration. The data points beyond $r = 0.7$ do not fall on this curve, however. This result implies that cooperative interaction with a binding constant $K_0\omega$ occurs at the singly contiguous site when 70% of the quaternary sites are bound to the dye molecules. Site–site interaction involving the doubly contiguous site in the high-saturation region ($0.7 < r \leq 1.0$) is not appropriate for the present system. This is possibly caused by steric hindrance imposed by the two bound dyes. Although the cooperativity effect may not persist in the high-saturation region involving the last one-third of the sites, the binding strength remains constant beyond $r = 0.7$. A linear Scatchard line with $n = 1$ and log $K = 5.2$ (see Figure 7) was used to approximate the experimental points.

The bound dye–dye interaction energy can be calculated from the parameter ω obtained in Figure 7, i.e., $-RT \ln \omega = -2.73$ kcal/mol. This value is smaller than the heats of dimerization for several larger planar aggregating dyes.[23] The heat of dimerization for the present dye is not available in the literature, mainly because the monomer and dimer peaks for the free dye in the UV–visible spectra are not greatly differentiated to allow spectrophotometric determination of the dimerization constant. Some preliminary NMR measurements[24] show that the dimerization constant of methyl orange in 0.01 M NaCl has approximately the same order of magnitude as the ω value estimated above. Consequently, we believe that the cooperative interaction caused by the bound dye–dye interaction originates from the aggregation tendency of the dye. Although aggregation occurs at a higher dye concentration in pure aqueous dye solution free of polymer, this effect may be manifested in the presence of polymer sites that can bring the dye molecules into proximity even at low dye concentration.

2. BPVI + MO. The data for BPVI + MO in 0.01 M NaAc and NaCl can be represented by linear Klotz or Scatchard plots, yielding $n = 1$, $K = 10^{6.3}$ (in 0.01 M NaCl)

and $n = 1$, $K = 10^{6.6}$ (in 0.01 M NaAc), respectively. Because the range for the extent of binding r is limited ($0.7 < r < 1.0$) for this strong binding polymer, the agreement between the calculated curves and the data points in these plots does not support the validity of the independent-site model, however.

One way to circumvent this difficulty was to increase the ionic strength of the medium to 0.05 M NaCl and hence to weaken the binding so that the data points can cover the whole range of r. These data were indeed obtained and analyzed in the same manner as those above for MPVI + MO and are summarized in Table IV. Direct comparison of the parameters K_0 and ω for the two polymer listed in this table is not appropriate because the two systems were not measured at the same ionic strength. Note that the cooperative model seems to describe well both systems when the polymer sites are approximately 70% occupied (i.e., $r = 0.6$–0.7).

Conclusions

1. The 1:1 stoichiometry for complexes of methyl orange and the quaternized poly(*N*-vinylimidazole) homopolymers suggests that binding capacity is dictated primarily by charge.

2. The binding strength between methyl orange and the quaternized polymers is influenced by (a) Coulombic interaction between the anionic dye and polycations, (b) nonionic interaction between the quaternizing side chain and the dye, and (c) nonionic bound dye–dye interaction.

3. The binding behavior in the saturation range $0 < r < 0.7$ can be described by the McGhee–von Hippel expression. The bound dye–dye interaction is associated with the aggregation tendency of the dye, which contributes an additional force to the overall polymer–dye interaction. The cooperative binding cannot persist, however, at a higher saturation level, possibly because of the steric hindrance of the two neighboring dye molecules.

Acknowledgment. We are grateful to Mrs. A. R. Sochor for technical assistance, Dr. I. S. Ponticello and Mr. K. R. Hollister for the preparation of some of the polymers used in this study, and Dr. H. Yu and Dr. J. L. Lippert for discussions during this study.

References and Notes

(1) Frank, H. S.; Evans, M. W. *J. Chem. Phys.* **1945**, *13*, 507.
(2) Kauzmann, W. *Adv. Protein Chem.* **1959**, *14*, 1.
(3) Franks, F. "Water, A Comprehensive Treatise"; Franks, F., Ed.; Plenum Press: New York, 1975; Vol. 4, p 1.
(4) Klotz, I. M.; Royer, G. P.; Sloniewsky, A. R. *Biochemistry* **1969**, *8*, 4752.
(5) Quadrifoglio, F.; Crescenzi, V. *J. Colloid Interface Sci.* **1971**, *35*, 447.
(6) Reeves, R. L.; Harkaway, S. A. "Micellization, Solubilization, and Microemulsions"; Mittal, K. L., Ed.; Plenum Press: New York, 1977; Vol. 2, p 819.
(7) Takagishi, T.; Nakata, Y.; Kuroki, N. *J. Polym. Sci.* **1974**, *12*, 807.
(8) Ando, Y.; Komiyama, J.; Iijima, T. *J. Chem. Soc. Jpn.* **1981**, *3*, 432.
(9) Tan, J. S.; Handel, T. M., to be submitted for publication.
(10) Orchard, B. J.; Tan. J. S.; Hopfinger, A. J. *Macromolecules* **1984**, *17*, 169.
(11) Tan, J. S.; Sochor, A. R. *Macromolecules* **1981**, *14*, 1700.
(12) Tan, J. S.; Gasper, S. P. *J. Polym. Sci. Polym. Phys. Ed.* **1974**, *12*, 1785.
(13) Scholtan, W. *Makromol. Chem.* **1953**, *11*, 131.
(14) Klotz, I. M. "The Proteins, Chemistry, Biological Activity, and Methods"; Neurath, H., Bailey, K., Eds.; Academic Press: New York, 1953; Vol. 1, p 727.
(15) Scatchard, G. *Ann. N.Y. Acad. Sci.* **1949**, *51*, 660.
(16) Tanford, C. "Physical Chemistry of Macromolecules"; Wiley: New York, 1967.
(17) von Hippel, P. H.; Schleich, T. *Acc. Chem. Res.* **1969**, *2*, 257.
(18) Cantor, C. R.; Schimmel, P. R. "Biophysical Chemistry"; W. H. Freeman: San Francisco, 1980; Part III.
(19) McGhee, J. D.; von Hippel, P. H. *J. Mol. Biol.* **1974**, *86*, 469.
(20) Schwarz, G. *Eur. J. Biochem.* **1970**, *12*, 442.
(21) Crothers, D. M. *Biopolymers* **1968**, *6*, 575.
(22) Hill, A. V. *J. Physiol. (London)* **1910**, *40*, iv.
(23) Coates, E. *J. Soc. Dyers Colour.* **1969**, *85*, 355.
(24) Hewitt, M.; Handel, T. M.; Tan, J. S., unpublished data.

Shape of Unperturbed Linear Polymers: Polypropylene

Doros N. Theodorou and Ulrich W. Suter*

Department of Chemical Engineering, Massachusetts Institute of Technology, Cambridge, Massachusetts 02139. *Received July 30, 1984*

ABSTRACT: Large numbers of conformations of unperturbed polypropylene chains are generated in Monte Carlo experiments, based on a rotational isomeric state scheme, and the average instantaneous shape in the system of principal axes of gyration is evaluated. Several new shape measures are introduced to characterize the shape anisotropy, asphericity, and acylindricity. Significant differences are found between short- and medium-length chains of different tacticity, while for long chains all shape measures converge to a common limit. The detailed three-dimensional segment density distributions are examined, and they are found to be bimodal along the longest principal axis of gyration. The loci of highest segment density are always two clearly separated domains, not containing the center of gyration, and they lie on the major principal axis separated by ca. $1.3\langle s^2\rangle_0^{1/2}$–$2.0\langle s^2\rangle_0^{1/2}$. The core of the segment distribution of an unperturbed chain is therefore dumbbell-like in shape.

Introduction

Flexible-chain molecules can assume a large number of conformations and shapes due to the many internal degrees of freedom. The *average shape* of these molecules is of importance for a variety of phenomena, especially for dilute-solution hydrodynamics. Commonly the segment distribution for long chains around their center of mass is examined as an average over all possible orientations in space, i.e., integrating over the external degrees of freedom, and spherical distributions of approximately Gaussian shape are obtained.[1-4] As early as 1934, however, Kuhn had realized[5] that the *instantaneous shape* of polymer coils, observed without orientational averaging, is far from spherical. Average shapes obtained without orientational averaging are therefore necessarily aspherical, and the accurate characterization of these shapes is relevant for the interpretation of phenomena with characteristic time scale smaller than the largest relaxation time of the

0024-9297/85/2218-1206$01.50/0